

Nonlinear optical properties of the mixture of ZnO nanoparticles and graphene nanosheets

Elmira Solati¹ · Davoud Dorrnian¹

Received: 21 November 2015 / Accepted: 24 January 2016 / Published online: 25 March 2016
© Springer-Verlag Berlin Heidelberg 2016

Abstract In this work, the experimental investigation of the nonlinear response of the mixture of ZnO nanoparticles and graphene nanosheets as a function of volumetric ratio of ZnO and graphene colloidal suspensions has been reported. The colloidal ZnO nanoparticle and graphene were synthesized by nanosecond pulsed laser ablation of Zn and graphite target in water, respectively. The X-ray diffraction pattern, transmission electron microscopy, Raman spectrum and linear absorption properties of ZnO nanoparticle and graphene nanosheets were used to characterize the ablation products. D band and G band of Raman shift at 1325 and 1580 cm^{-1} , respectively, confirmed the formation of graphene nanosheets in water. Results show that the bandgap energy of mixtures decreased noticeably with increasing the amount of graphene in the suspensions. The nonlinear optical properties of the mixture of ZnO nanoparticles and graphene nanosheets were also investigated using open and close z-scan experiments. The positive nonlinear refractive index and absorption coefficient of the mixture of graphene nanosheets and ZnO nanoparticles were increased with increasing the concentration of graphene in the mixtures.

1 Introduction

Graphene, a single layer of carbon in a hexagonal lattice demonstrates many interesting electrical and optical properties that appear due to its zero bandgap energy. Compared to other carbon nanostructures like fullerenes, carbon nanotubes

and graphite, the interest in graphene-based materials has been exponentially increased due to its unique properties like high carrier mobility at room temperature, large specific surface area, good optical transparency and thermal conductivity. Graphene and graphene oxide have significant and important nonlinear optical (NLO) properties [1]. Graphene has unique absorption properties. Such unique absorption could become saturated when the input optical intensity is above a threshold value. Graphene can be saturated readily under strong excitation over the visible to near-infrared region, due to the universal optical absorption and zero bandgap. This has relevance for the mode locking of fiber lasers, where fullband mode locking has been achieved by graphene-based saturable (SA) absorber. Due to this special property, graphene has wide application in ultrafast photonics. Moreover, the optical response of graphene and graphene oxide layers can be tuned electrically [2–4]. Saturable absorption in graphene could occur at the microwave and terahertz band, owing to its wideband optical absorption property. The microwave saturable absorption in graphene demonstrates the possibility of graphene microwave and terahertz photonics devices, such as microwave saturable absorber, modulator, polarizer, microwave signal processing and broadband wireless access networks [5]. Under more intensive laser illumination, graphene could also possess a nonlinear phase shift due to the optical nonlinear Kerr effect [6, 7].

It has been demonstrated that graphene incorporated with nanoparticles exhibits high activity for catalytic applications, including photocatalytic reduction, solar cells and fuel cells. These advanced functions can be due to the electron transfer from the conduction band of semiconductor to the graphene [8]. Zinc oxide (ZnO) also is a semiconductor with a great application potential in optics. Compared with other semiconductor materials, ZnO with a wide and direct bandgap of 3.37 eV has higher exciton binding energy

✉ Davoud Dorrnian
d.dorrnian@gmail.com; doran@srbiau.ac.ir

¹ Laser Lab., Plasma Physics Research Center, Science and Research Branch, Islamic Azad University, Tehran, Iran

(60 meV) and has been studied as an optoelectronic, transparent conducting and piezoelectric material [9–11]. Taking into consideration the excellent properties of ZnO and graphene, the mixture of ZnO nanoparticles and graphene nanosheets can enable multi-purpose properties with competence far beyond those of the individual members.

Recently, there has been a growing interest in fundamental and experimental studies focused on NLO properties of graphene/ZnO composites. Kavitha et al. [1] worked on synthesis of reduced graphene oxide–ZnO hybrid with enhanced optical limiting property. They found that there was a 15 times enhancement in nonlinear absorption coefficient of the reduced graphene oxide/ZnO hybrid compared to bare ZnO. Ouyang et al. [12] have worked on enhanced nonlinear optical and optical limiting properties of graphene/ZnO hybrid organic glasses. Their results showed that the graphene/ZnO/poly methyl methacrylate organic glasses exhibited enhanced nonlinear absorption and nonlinear scattering properties compared to the ZnO/PMMA organic glass, resulting in excellent optical limiting performance. Song et al. [13] worked on synthesis and nonlinear optical properties of reduced graphene oxide hybrid material covalently functionalized with zinc phthalocyanine. Their results showed that NLO properties and optical limiting performance of the reduced graphene oxide/zinc phthalocyanine hybrid increased noticeably in comparison with individual graphene oxide, zinc phthalocyanine and the graphene oxide–zinc phthalocyanine hybrid.

Their results were extracted from the simple but precise z-scan experiment data for measuring the nonlinear refractive index and absorption coefficient. Z-scan technique is a simple and popular experimental technique to measure intensity-dependent nonlinear susceptibilities of materials, way to obtain information of nonlinear refractive index and nonlinear absorption properties of materials [14–18]. In most experiments, Q-switched Nd:YAG laser was used as the source to induce nonlinearity in their samples, but in our z-scan measurement for the first time, the second harmonic continuous wave Nd:YAG laser was used. NLO behavior of materials strongly depends on the intensity of the incident beam. Our results show that in the low energy regime, the nonlinear absorption of ZnO nanoparticles/graphene nanosheets mixture is based on saturable absorption and we may increase the nonlinearity of mixture with increasing the amount of graphene nanosheets.

2 Experimental

2.1 Synthesis of graphene nanosheets and ZnO nanoparticles

Graphene nanosheets were produced by pulsed laser ablation of a graphite plate (99.9 % purity) in water. Graphite

target was irradiated with the fundamental wavelength (1064 nm) of a pulsed Nd:YAG laser operated at 7 ns pulse width and 5 Hz repetition rate. In water environment, 5000 laser pulse was used to produce graphene nanosheets. The fluence of laser pulse was 0.7 J/cm^2 with 6 mm diameter, which was focused by a 80-mm focal length lens on the surface of the target. Graphite target was placed on the bottom of an open glass cylindrical vessel filled with 80 ml distilled water. Height of liquid on the target was 0.8 cm. ZnO nanoparticles were produced using the same system. The fluence of the laser pulse for producing ZnO nanoparticles was 0.5 J/cm^2 . Both targets and containers were cleaned ultrasonically in alcohol, acetone and deionized water before the experiments.

2.2 Synthesis of graphene/ZnO composites

The produced graphene and ZnO suspensions were mixed in different volumetric ratio. We mixed graphene/ZnO suspensions at the volume ratio of 1/2 (sample 1), 1/1 (sample 2), 3/2 (sample 3), and 2/1 (sample 4). Twenty milliliters of ZnO nanoparticles suspension was mixed with 10, 20, 30 and 40 ml of graphene nanosheet suspension in samples 1–4, respectively. Then these mixtures were sonicated for 2 h to get a uniform dispersion. Pictures of graphene and ZnO suspensions and mixture of ZnO nanoparticles/graphene suspensions are presented in Fig. 1. After ablation the color of ZnO nanoparticles suspension was light brown and the color of graphene suspension was light gray.

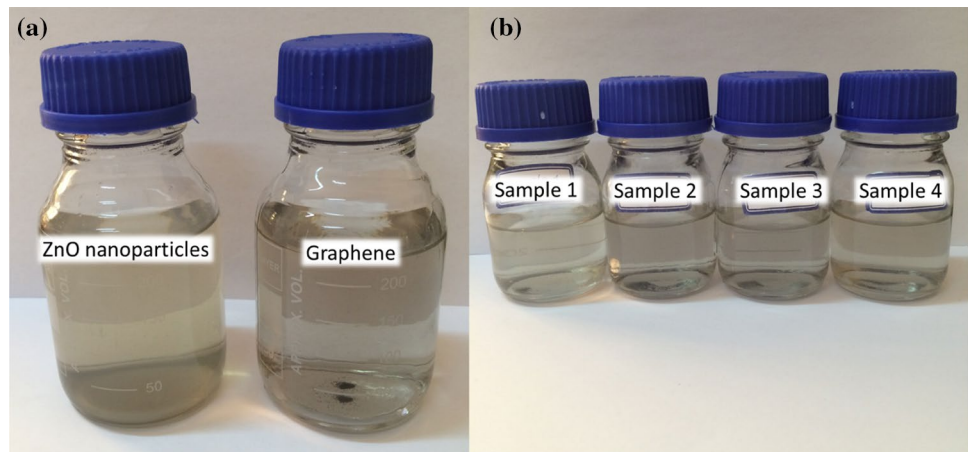
2.3 Characterization

A variety of analytical techniques were employed for characterization of products. The optical properties of suspensions were examined at room temperature by UV–Vis–NIR spectrophotometer from PG instruments Ltd. The crystalline structure of the dried ZnO nanoparticles and graphene nanosheets suspensions on silicon substrate was analyzed using a Cu-K α radiation ($\lambda = 1.54060 \text{ \AA}$) of STOE–XRD diffractometer. Zeiss EM10C transmission electron microscope was employed to investigate the size and form of the ZnO nanoparticles and graphene nanosheets. For transmission electron microscopy (TEM) imaging, few drops of the concentrated suspensions were dried on a carbon-coated copper grid. Raman Thermo Nicolet disperse spectroscope from Almega was utilized to determine the structure, quality and amount of produced graphene in suspensions. To perform Raman spectra, few drops of suspensions were dried on glass substrate.

2.4 Nonlinear optical properties measurement

Open and close z-scan experiments were carried out to study the nonlinear optical properties of samples. In the

Fig. 1 ZnO nanoparticles and graphene nanosheets suspensions produced by laser ablation (a) and mixture of ZnO nanoparticles and graphene nanosheets (b)



z-scan measurement system, a 100 mW second harmonic continuous wave Nd:YAG laser of 532 nm wavelength was used as the source to induce nonlinearity in samples. During the exposure, sample was mounted on a controlled translation stage and it was moved along the z -axis through the focal point of a lens of 10-mm focal length. The radius of the beam waist of laser was 1 mm before the lens and was calculated to be 20 μm at the focus. Colloidal samples were taken in 1 mm thickness quartz cuvette, which were placed at the axis of the beam and scanned on either side of focal point. In the closed z -scan experiment, the diameter of the aperture was 0.5 mm.

3 Results and discussion

3.1 Structural characterization of the ZnO nanoparticles and graphene sheets

The crystalline structures of ZnO nanoparticles and Zn target were characterized by X-ray diffraction, which are shown in Fig. 2. The peak at $2\theta = 69.41^\circ$ in the ZnO nanoparticles X-ray pattern is due to silicon substrate lattice structure. Various peaks of ZnO XRD pattern are corresponded to the hexagonal wurtzite phase of ZnO. The main dominant peaks of ZnO nanoparticles were identified at $2\theta = 31.81^\circ$, 34.51° , 36.31° , 47.61° , 56.71° , and 63.11° . The XRD peaks of nanoparticles are different from Zn target peaks. It can be concluded that Zn and O atoms are composed randomly during the ablation process. Ablation of Zn atoms produced local high-temperature and high-pressure plasma plume and nucleation was occurred during the plasma plume expansion phase on the surface of Zn target. Chemical reaction and physical processes took place between the ablated Zn target and water molecules, which caused the formation of ZnO nanoparticles in the water environment. Same results were reported in our previous work [10].

Figure 3 shows the X-ray diffraction pattern of the produced graphene nanosheets and graphite target. The disappearance of graphite target XRD peaks in the XRD pattern of as-prepared graphene sample in water supports the formation of graphene sheets [19, 20]. Basically the peaks in XRD diffraction pattern of materials are the reflected X-ray photons from the atoms on the successive planes of their lattice, which satisfy the Bragg's condition. When the number of plane is small, we may not expect large reflection of X-ray photons. In this case, we will not have strong peaks in the XRD pattern of graphene. This result is in good agreement with the result of TEM image.

TEM images of the ZnO nanoparticles, graphene and mixture of ZnO nanoparticles and graphene are displayed in Fig. 4. Most of the ZnO nanoparticles with an average diameter of about 29.5 nm are spherical with some hexagonal shape particles between them. The micrograph of graphene shows a sheetlike transparent morphology. We may observe the folded regions over the graphene sheet. The high transparency of TEM image of graphene confirms that they are few layers graphene. It can be clearly seen in the TEM image of the mixture of ZnO nanoparticles and graphene sheets that the exfoliated graphene sheet was decorated with ZnO nanoparticles.

3.2 Raman spectrum

The Raman spectrum of graphene in the range of 1200–1700 cm^{-1} is presented in Fig. 5a. Data have been recorded from the dried drops of graphene suspension on a glass substrate with 0.1 cm^{-1} spectral resolution.

According to the literature the D band at 1325 cm^{-1} and the G band at 1580 cm^{-1} are attributed to the graphene in this sample [21–23]. With increasing the local defects in the graphene, the intensity of D band increases. In this work, the ratio of the integrated intensity of the disorder-induced D band to that of the G band is small. The small

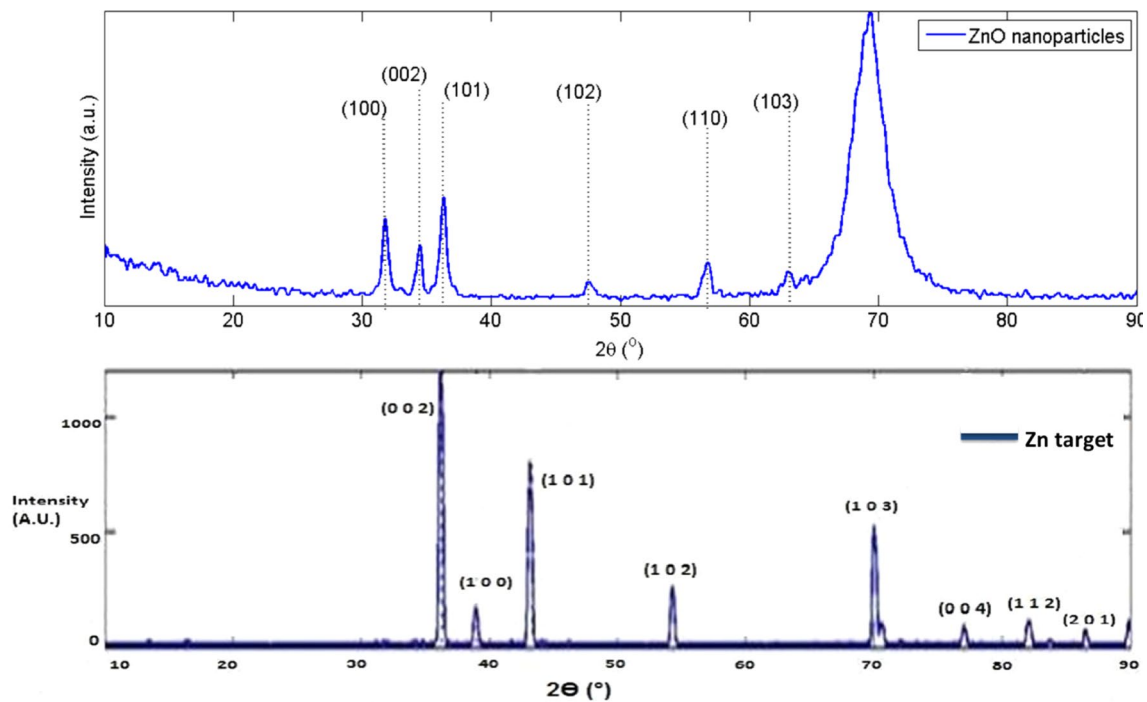
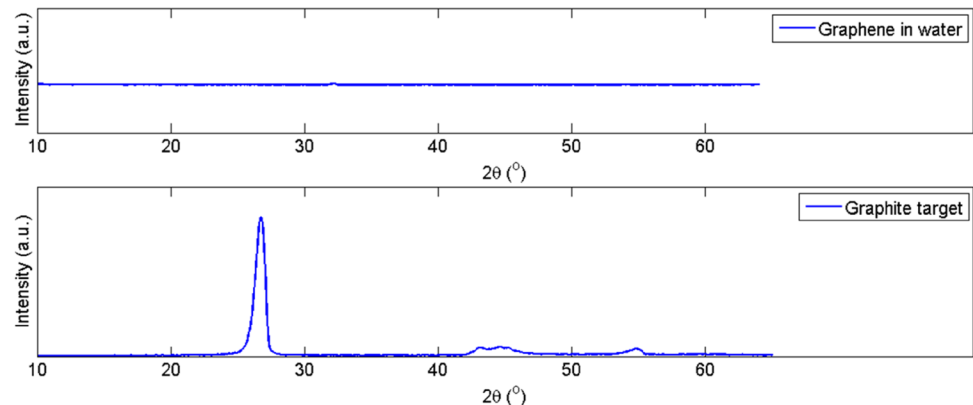


Fig. 2 X-ray diffraction patterns of ZnO nanoparticles and Zn target

Fig. 3 X-ray diffraction patterns of graphene and graphite target



magnitude of I_D/I_G indicates the increased fraction of sp^2 domains and decreased defect in this sample and suggests an acceptable quality of graphene nanosheets in the suspension. In order to determine the average domain size of the sp^2 in graphene, we employed the Tuinstra and Koenig relation, which relates the ratio of D and G bands intensities into the crystallite size as follows [24];

$$\frac{I_D}{I_G} = \frac{2 \times 10^{-10} (\lambda^4)}{L} \quad (1)$$

where L is sp^2 domain size, λ is the laser wavelength which was used for Raman spectroscopy, and I_D/I_G is the intensity ratio of the D and G peaks. In this work, the calculated value of sp^2 domain size is 8.04 nm. The G band

intensity is high due to the increase in the sp^2 domain in graphene [25]. In other reports, the calculated values of sp^2 domain size in graphene oxide and in graphene are about 12.08–16.28 and 14–26 nm, respectively, while the calculated values of sp^2 domain size in reduced graphene oxide is 6.77 nm [26–28].

Figure 5 (b) displays the Raman shift due to the dried graphene suspension in the range of 1000–3000 cm^{-1} . The 2D band is occurred at 2678 cm^{-1} in the spectrum, due to production of graphene. Because of added forces from the interactions between layers of AB-stacked graphene, as the number of graphene layers increases, the spectrum will change from that of single-layer graphene, namely a splitting of the 2D peak into an increasing number of modes

Fig. 4 TEM images of ZnO nanoparticles, graphene and mixture of ZnO nanoparticles and graphene

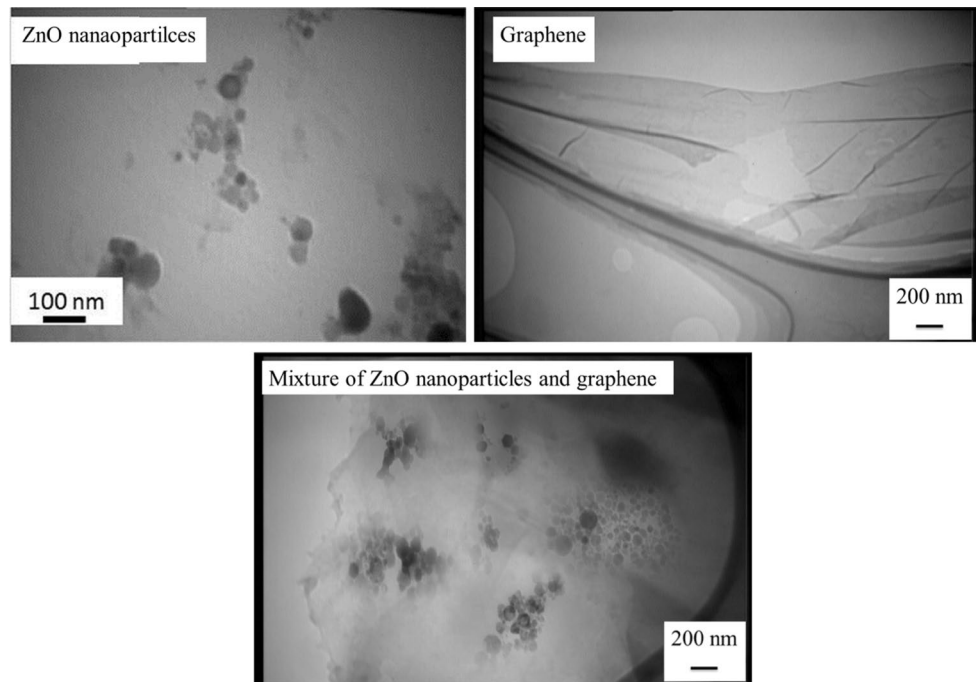
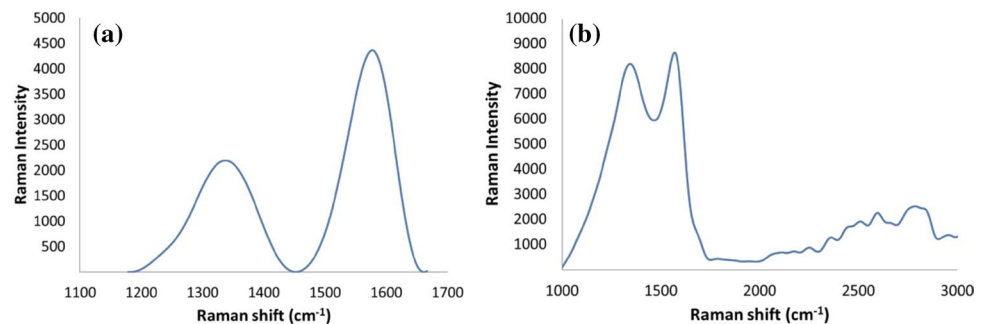


Fig. 5 Raman scattering spectrum of graphene in the range of **a** 1200–1700 cm^{-1} and **b** 1000–3000 cm^{-1}



that can combine to give a wider, shorter, higher-frequency peak [22]. A characteristic peak generally named G' ($\sim 2950 \text{ cm}^{-1}$) was found in the spectrum due to the graphite-based materials.

3.3 UV–Vis–NIR absorption spectra

The UV–Vis–NIR absorption spectra of samples are illustrated in Fig. 6. By applying sonication at the mixing step, significant breakup of nanoparticles agglomerated and penetration of ZnO nanoparticles between graphene sheets took place. When the mixture of ZnO nanoparticles and graphene suspension was exposed to the ultrasonic irradiation, bubbles grew in it. Bubbles collapsed when they reached maximum size. This strong collapse raised the temperature and caused the rupture of chemical bonds led to formation of free radicals [29]. The absence of absorption edge can be seen in the absorption spectra of these samples before sonication. However, after ultrasonic,

the absorption edge was formed in the range of 329–340 nm. The intensity of absorption peak was increased by sonication.

Figure 7 shows the UV–Vis–NIR absorption spectra of ZnO nanoparticles, graphene sheets and samples after applying ultrasonic irradiation. The spectrum of the ZnO nanoparticles showed exciton absorption at 308 nm. The broad UV absorption band at 309–347 nm can be attributed to the combination of the band of ZnO nanoparticles and π – π^* transition of C=C bands of graphene. The slight red shift of absorption peak and change in the width of UV absorption band of the mixture spectra in comparison with the ZnO spectrum suggests the ground-state electronic interactions between the ZnO nanoparticles and graphene. Moreover, in comparison with the pure graphene sheets, the UV absorption intensity of samples was increased, while the absorption of samples was smaller than ZnO nanoparticles. In addition, it is noticeable that there was a reduction in absorption intensity with

Fig. 6 UV–Vis–NIR absorption spectra of samples before and after ultrasonic

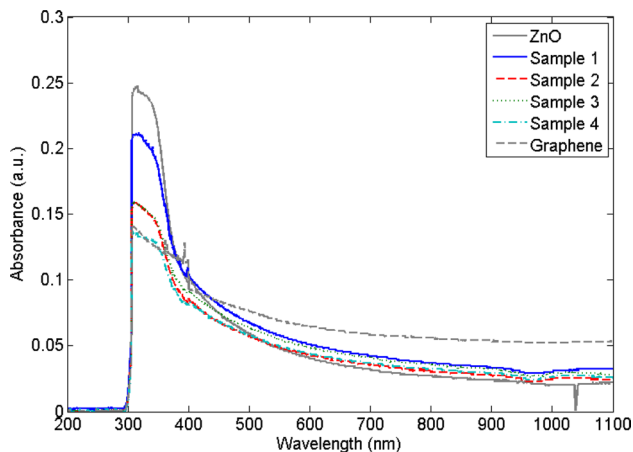
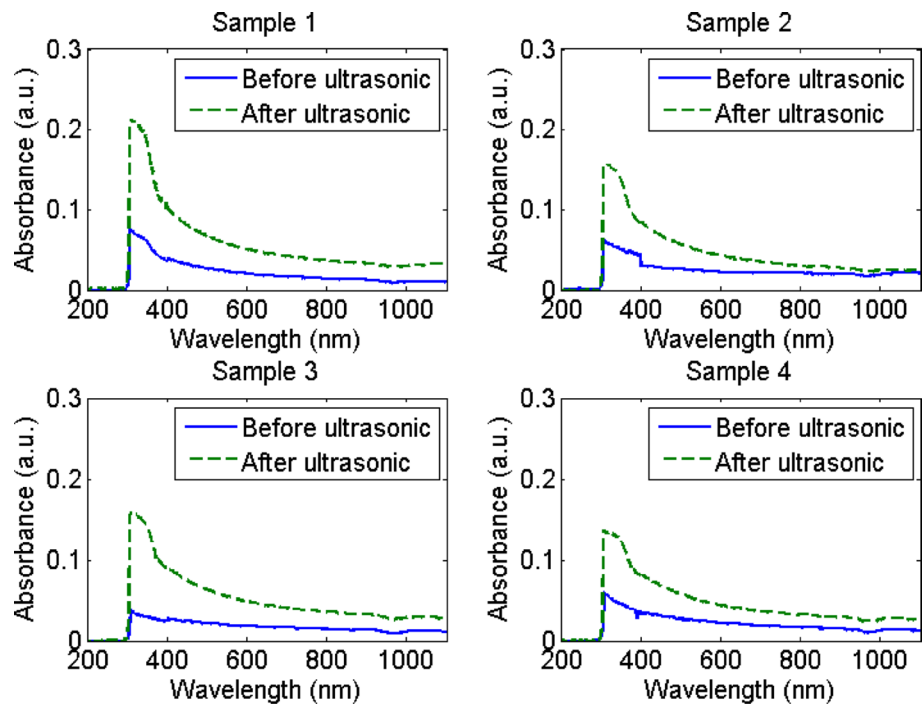


Fig. 7 UV–Vis–NIR absorption spectra of ZnO nanoparticles, graphene sheets and mixture samples after ultrasonic irradiation

increasing the concentration of graphene in the samples and its intensity depended on the amount of graphene in the suspensions.

By using the Tauc's equation, the optical bandgap can be obtained from absorption coefficient. Absorption coefficient of ZnO nanoparticles, graphene nanosheets and samples is evaluated from their transmittance spectrum using the following relation [30]:

$$\alpha = -\frac{1}{d} \ln \left(\frac{I}{I_0} \right) \quad (2)$$

where α is the absorption coefficient and d is the thickness of samples, which was taken 1 cm, equal to the thickness of quartz cuvette of spectrometer. I and I_0 are the intensities of transmitted and incident beam, respectively. The Tauc's equation can be written as [31]:

$$(\alpha h\nu) = A(h\nu - E_g)^m \quad (3)$$

Here, A is a constant that depends on the transition, $h\nu$ is the photon energy and the type of transition can be obtained finding the value of m . The parameter m has the value 1/2 for the direct allowed transition but in forbidden cases it is 3/2 and the value 2 is for the indirect allowed transition and for the forbidden cases it is 3 or more [32]. For allowed direct transition, Fig. 8 exhibits the derived spectra for the relationship of $(\alpha h\nu)^2$ versus photon energy $h\nu$. Values of the optical energy gap E_g were determined from the intercept of the extrapolation of the linear part to zero absorption with the photon energy axis. Using this method the optical bandgap value obtained for ZnO nanoparticles was 3.32 eV and the optical bandgap energy for samples 1–4 was found to be 3.18, 3.15, 3.12 and 3.11 eV, respectively. According to the result with increasing the amount of graphene in the suspensions, the bandgap energies of samples were decreased.

Pure graphene has a zero bandgap and thus behaves like a metal. Results show that the bandgap energy of mixture of ZnO nanoparticles and graphene was smaller than the bandgap of ZnO nanoparticles and increasing the amount of graphene decreased the bandgap energy of samples.

Fig. 8 Direct bandgap calculation of ZnO nanoparticles and samples

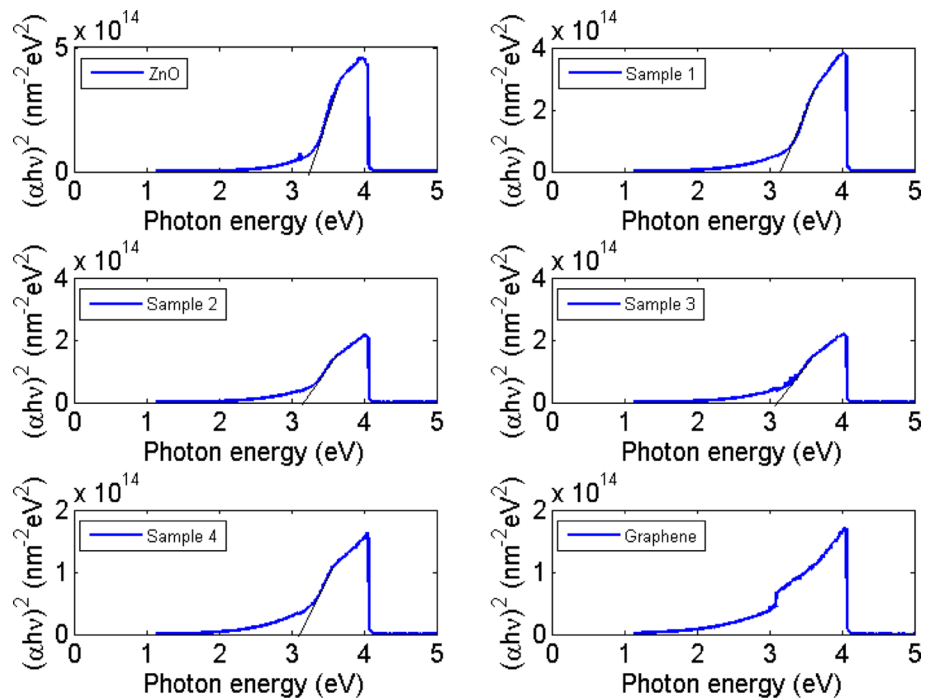
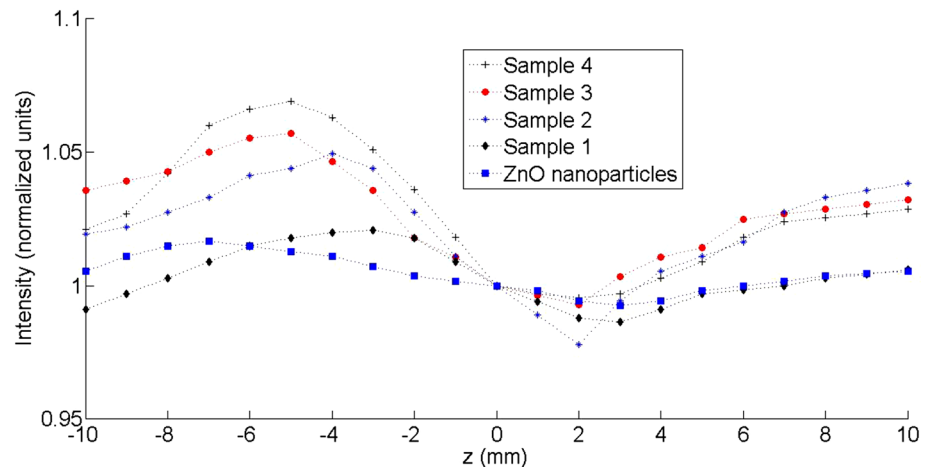


Fig. 9 Closed aperture z-scan data



3.4 Open and close z-scan

In the z-scan technique, one measures the change in the intensity of a focused beam as a sample travels axially (the z -axis) through the beam waist with $z = 0$ at the focal plane. There are two variations of z-scan, each of which yields a different component of $\chi^{(3)}$. The closed aperture z-scan gives the real component of $\chi^{(3)}$ corresponds to nonlinear refraction; and the open aperture z-scan determines the imaginary component of $\chi^{(3)}$ corresponds to nonlinear absorption.

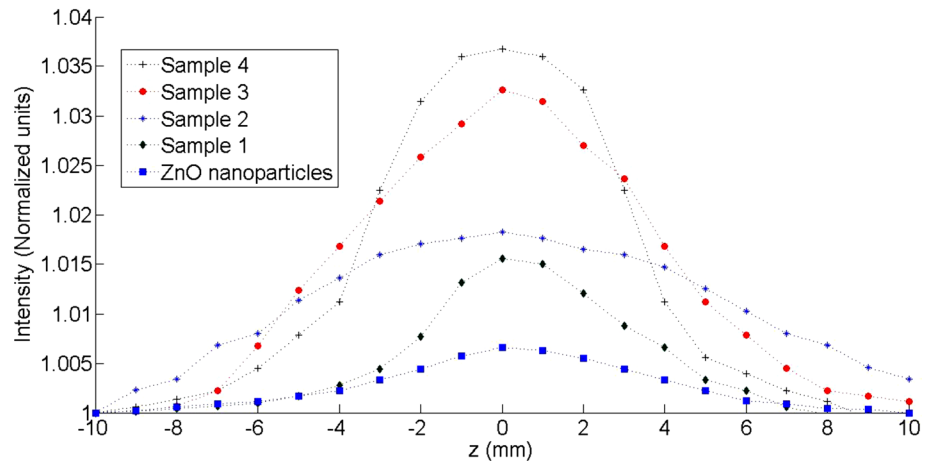
Figure 9 shows the normalized transmittance of closed aperture z-scan as a function of distance from the focus point of the Gaussian beam ($z = 0$). Any other material was

not chosen as the reference. According to a pair of simple equations; $d(\Delta\varphi)/dz = \Delta n(I) k$ and $dI/dz = -\alpha(I) I$, where k is the wave vector. In the propagation depth in the samples for Gaussian beam, the nonlinear refraction is related to the on-axis phase shift $\Delta\varphi$ at the focus and $\alpha(I)$ includes linear and nonlinear absorption terms [33].

When the data of normalized transmittance in closed aperture z-scan show a perfect symmetry curves, the absorption coefficient is very small so the open aperture z-scan curves for the hypothetical sample are linear. In general, the peak and the valley of the closed aperture z-scan are asymmetric due to both the axial phase shift $\Delta\varphi_0$ and the nonlinear absorption [33–36]. The nonlinear refractive index can be calculated from the normalized transmittance

Table 1 Magnitudes of ΔT_{p-v} , $\Delta\varphi_0$, α , L_{eff} and n_2 of ZnO nanoparticles and samples

Sample	ΔT_{p-v}	$\Delta\varphi_0$	α (mm ⁻¹)	L_{eff} (mm)	$n_2 \times 10^{-13}$ (m ² /W)
ZnO nanoparticles	0.0244	0.0678	1.1	0.6065	1.183
Sample 1	0.0324	0.0900	1.2	0.5823	1.635
Sample 2	0.0710	0.1972	1.3	0.5596	3.728
Sample 3	0.0741	0.2058	1.4	0.5381	4.046
Sample 4	0.0750	0.2083	1.5	0.5179	4.255

Fig. 10 Open aperture z-scan data

data of closed aperture measurement, which can be written as follows [33]:

$$\Delta T_{p-v} = 0.406(1 - S)^{0.25} \Delta\varphi_0 (\Delta\varphi_0 \leq \pi) \quad (4)$$

where $\Delta T_{p-v} = T_p - T_v$ is the difference between normalized peak and valley transmittance, $S = 1 - \exp(-2r_A^2/w_A^2)$ is the aperture linear transmittance with r_A denoting the radius of aperture and w_A denoting the beam radius at the aperture in the linear region and $\Delta\varphi_0$ is the induced phase distortion of radiation passed through the sample. The nonlinear refractive index n_2 can be finally calculated by the following equation [33]:

$$n_2 = \frac{\lambda \Delta\varphi_0}{2\pi I_0 L_{\text{eff}}} \quad (5)$$

where $L_{\text{eff}} = (1 - \exp(-\alpha L))/\alpha$ is known as the effective thickness of the sample, L is the thickness of the cell, λ is the laser wavelength, $I_0 = 8 \times 10^7$ W/m² is the Gaussian beam intensity at the focal plane, and α is the linear absorption coefficient when $\lambda = 532$ nm.

The calculated values of the nonlinear refractive index for the samples 1–4 and ZnO nanoparticles are listed in Table 1. We observed that the nonlinear refractive index increased with increasing the concentration of the graphene nanosheets in the samples. Increasing the concentration of graphene led to increase the numbers of nanostructures in effective thickness, so the interaction of nanostructures

which were located in the beam path with laser beam enhanced. By increasing these interactions, the nonlinear refractive index was increased. The rate of increasing in nonlinear refractive index was not same for all samples. The variation of ΔT_{p-v} is a function of $\Delta\varphi_0$, for a specific aperture size. In this case, ΔT_{p-v} was increased with increasing the concentration of graphene in samples.

Figure 10 shows the results of open aperture z-scan experiments. Transmission at the focus was increased with increasing the concentration of graphene in samples. Sample transmittance was increased with input laser intensity (intensity is maximum at the focal point $z = 0$ and decreases gradually in both $+z$ and $-z$ directions), suggesting a SA behavior. It indicated that the SA of samples could be enhanced by increasing the concentration of graphene. Actually the higher concentration of the graphene gives stronger NLO properties [37].

Since the laser beam was single TEM₀₀ Gaussian beam, we can use Eq. 6 to calculate the normalized transmittance for the open aperture condition;

$$T(z, s = 1) = \sum_{m=0}^{\infty} \frac{[-q_0(z)]^m}{(m+1)^{3/2}} \quad (6)$$

For $q_0 < 1$, where

$$q_0(z) = \frac{I_0 L_{\text{eff}} \beta}{\left(1 + \frac{z^2}{z_0^2}\right)} \quad (7)$$

Table 2 Magnitudes of $T(z, s = 1)$, q_0 , β , and $\chi^{(3)}$ of ZnO nanoparticles and samples

Sample	$T(z, s = 1)$	q_0	$\beta \times 10^{-2}$ (m/W)	$\text{Re}\chi^{(3)} \times 10^{-15}$ (SI)	$\text{Im}\chi^{(3)} \times 10^{-14}$ (SI)	$ \chi^{(3)} \times 10^{-14}$ (SI)
ZnO nanoparticles	0.007	2.8086	0.005789	0.7440	1.543	1.544
Sample 1	0.016	2.7831	0.005974	1.0290	1.592	1.595
Sample 2	0.018	2.7775	0.006204	2.3466	1.654	1.670
Sample 3	0.033	2.7351	0.006353	2.5466	1.693	1.712
Sample 4	0.037	2.7237	0.006574	2.6782	1.752	1.772

where $z_0 = k\omega_0^2/2$ is the diffraction length of the focused beam. Similar to closed aperture experiments, the laser beam intensity of $I_0 = 8 \times 10^7 \text{ W/m}^2$ was used in this part. The calculated values of β are presented in Table 2. Numerical values are indicative of increased nonlinear absorption at the focus with increasing the concentration of graphene in samples. Thus, this nanomaterial could be a good candidate for nonlinear optical devices. Mixture of ZnO nanoparticles and graphene nanosheets shows significant increase in nonlinear absorption, which in turn may be due to increase in the extended conjugation on the graphene nanosheets compared to that of pure ZnO nanoparticles. Also it may be due to saturable absorption and photoinduced photon transfer between ZnO and graphene nanosheets. Importantly, the values of the NLO parameters can be controlled by adjusting the volumetric ratio of mixture of ZnO nanoparticles and graphene. If the added amount of graphene increases, the values of the NLO parameters will also increase.

In electromagnetism, the electric susceptibility is a dimensionless proportionality coefficient that indicates the degree of polarization of a dielectric material in response to an applied electric field. In many materials, the polarizability starts to saturate at high values of electric field. This saturation can be modeled by a nonlinear susceptibility [38]. The real and imaginary parts of the third-order nonlinear optical susceptibility $\chi^{(3)}$ in the international system (SI) of units are the following equations [39]:

$$\text{Re}\chi^{(3)} = \left(\frac{4}{3}\right)n_0^2\varepsilon_0cn_2 \tag{8}$$

And

$$\text{Im}\chi^{(3)} = \left(n_0^2\varepsilon_0c\lambda/3\pi\right)\beta \tag{9}$$

where n_0 , ε_0 , c , and λ denote, respectively, the linear refractive index of the material, the electric permittivity of free space ($8.85 \times 10^{-12} \text{ F/m}$), the speed of light in the vacuum and the wavelength.

Based on this theory, results of experiments are used to calculate $\text{Re}\chi^{(3)}$ and $\text{Im}\chi^{(3)}$, which are presented in Table 2. The values of $\text{Re}\chi^{(3)}$ and $\text{Im}\chi^{(3)}$ increase with

increasing the concentration of graphene in samples. Thus, the absolute value of the third-order nonlinear optical susceptibility was calculated as:

$$|\chi^{(3)}| = \left[\left(\text{Re}\left(\chi^{(3)}\right)\right)^2 + \left(\text{Im}\left(\chi^{(3)}\right)\right)^2\right]^{1/2} \tag{10}$$

The values of the third-order nonlinear susceptibility obtained for the present samples are listed in Table 2.

Saturable absorption is an important nonlinear optical property of graphene. When graphene is under laser irradiance, the electrons in lower energy states absorb the energy of photons and jump to higher energy states. However, when the laser intensity is so high that most of the higher electron energy states are occupied, and hence, further absorption is blocked, which is known as ‘‘Pauli blocking’’ effect. This results in saturable absorption of graphene [3].

4 Conclusions

We have reported the synthesis, and nonlinear optical properties of the mixture of ZnO nanoparticles and graphene nanosheets. The results of XRD, Raman, UV–Vis–NIR and morphological studies of TEM confirm the successful fabrication of ZnO nanoparticles and graphene sheets. Slight red shift and change in the width of absorption peak of the mixture samples compare to the ZnO nanoparticles suggest the ground-state electronic interactions between the ZnO nanoparticles and graphene nanosheets. Increasing the amount of graphene in mixtures decreased the band-gap energy of samples. This is a suitable way to decrease the bandgap energy of ZnO and expands its applications. In conclusion, from nonlinear optical measurements conducted in the mixture of ZnO nanoparticles and graphene nanosheets we showed that their nonlinear refractive index and absorption behavior can be tailored by controlling the concentration of graphene. Compare to ZnO nanoparticle, the mixture of ZnO nanoparticles and graphene nanosheets exhibits good nonlinear absorption, which may be due to the saturable absorption.

References

- M.K. Kavitha, H. John, P. Gopinath, R. Philip, Synthesis of reduced graphene oxide–ZnO hybrid with enhanced optical limiting property. *J. Mater. Chem. C* **1**, 3669–3676 (2013)
- U. Kurum, B. Liu, K. Zhang, Y. Liu, H. Zhang, Electrochemically tunable ultrafast optical response of graphene oxide. *Appl. Phys. Lett.* **98**, 141103 (2011)
- Q. Bao, H. Zhang, Y. Wang, Z. Ni, Y. Yan, Z. Shen, K.P. Loh, D.Y. Tang, Atomic-layer graphene as a saturable absorber for ultrafast pulsed lasers. *Adv. Funct. Mater.* **19**, 3077–3083 (2009)
- H. Zhang, D. Tang, R.J. Knize, L. Zhao, Q. Bao, K.P. Loh, Graphene mode locked, wavelength-tunable, dissipative soliton fiber laser. *Appl. Phys. Lett.* **96**, 111112 (2010)
- Z. Zheng, C. Zhao, S. Lu, Y. Chen, Y. Li, H. Zhang, S. Wen, Microwave and optical saturable absorption in graphene. *Opt. Express* **20**, 23201–23214 (2012)
- H. Zhang, S. Virally, Q. Bao, K.P. Loh, S. Massar, N. Godbout, P. Kockaert, Z-scan measurement of the nonlinear refractive index of graphene. *Opt. Lett.* **37**, 1856–1858 (2012)
- H. Dong, C. Conti, A. Marini, F. Biancalana, Terahertz relativistic spatial solitons in doped graphene metamaterials. *J. Phys. B At. Mol. Opt. Phys.* **46**, 15540 (2013)
- B. Li, H. Cao, ZnO@graphene composite with enhanced performance for the removal of dye from water. *J. Mater. Chem.* **21**, 3346–3349 (2011)
- D. Dorrnian, E. Solati, L. Dejam, Photoluminescence of ZnO nanoparticles generated by laser ablation in deionized water. *Appl. Phys. A* **109**, 307–314 (2012)
- E. Solati, L. Dejam, D. Dorrnian, Effect of laser pulse energy and wavelength on the structure, morphology and optical properties of ZnO nanoparticles. *Opt. Laser Technol.* **58**, 26–32 (2014)
- A. Mehrani, D. Dorrnian, E. Solati, Properties of Au/ZnO nanocomposite prepared by laser irradiation of the mixture of individual colloids. *J. Clust. Sci.* **26**, 1743–1754 (2015)
- Q. Ouyang, Z. Xu, Z. Lei, H. Dong, H. Yu, L. Qi, C. Li, Y. Chen, Enhanced nonlinear optical and optical limiting properties of graphene/ZnO hybrid organic glasses. *Carbon* **67**, 214–220 (2014)
- W. Song, C. He, W. Zhang, Y. Gao, Y. Yang, Y. Wu, Z. Chen, X. Li, Y. Dong, Synthesis and nonlinear optical properties of reduced graphene oxide hybrid material covalently functionalized with zinc phthalocyanine. *Carbon* **77**, 1020–1030 (2014)
- R.L. Dantec, Y. Mugnier, G. Djanta, L. Bonacina, J. Extermann, L. Badie, C. Joulaud, M. Gerrmann, D. Rytz, J.P. Wolf, C. Galez, Ensemble and Individual characterization of the nonlinear optical properties of ZnO and BaTiO₃ nanocrystals. *J. Phys. Chem. C* **115**, 15140–15146 (2011)
- R. Sreeja, J. John, P.M. Aneesh, M.K. Jayaraj, Linear and nonlinear optical properties of luminescent ZnO nanoparticles embedded in PMMA matrix. *Opt. Commun.* **283**, 2908–2913 (2010)
- Y. Golian, M. Rashidian, D. Dorrnian, Effect of ultraviolet (UV) light treatment on the nonlinear optical properties of red lake doped polyvinyl chloride (PVC) film. *Lasers Eng. (Old City Publishing)* **29**, 69–82 (2014)
- M. Rashidian, D. Dorrnian, Effect of concentration on the plasmonic absorption and optical nonlinearity of gold nanoparticles. *Opt. Eng.* **51**, 089001 (2012)
- M. Rashidian, M. Ghoranneviss, D. Dorrnian, Thermo optical properties of Ag nanoparticles produced by pulsed laser ablation. *Opt. Quant. Electron.* **47**, 3729–3745 (2015)
- K. Awasthi, R. Kumar, H. Raghubanshi, S. Awasthi, R. Pandey, D. Singh, T.P. Yadav, O.N. Srivastava, Synthesis of nano-carbon (nanotubes, nanofibres, graphene) materials. *Bull. Mater. Sci.* **34**, 607–614 (2011)
- Q. Du, M. Zheng, L. Zhang, Y. Wang, J. Chen, L. Xue, W. Dai, G. Ji, J. Cao, Preparation of functionalized graphene sheets by a low-temperature thermal exfoliation approach and their electrochemical supercapacitive behaviors. *Electrochim. Acta* **55**, 3897–3903 (2010)
- N.R. Wilson, P.A. Pandey, R. Beanland, R.J. Young, I.A. Kinloch, L. Gong, Z. Liu, K. Suenaga, J.P. Rourke, S.J. York, J. Sloan, Graphene oxide: structural analysis and application as a highly transparent support for electron microscopy. *ACS Nano* **3**, 2547–2556 (2009)
- S.Z. Mortazavi, P. Parvin, A. Reyhani, Fabrication of graphene based on Q-switched Nd:YAG laser ablation of graphite target in liquid nitrogen. *Laser Phys. Lett.* **9**, 547–552 (2012)
- J.E. Proctor, E. Gregoryanz, K.S. Novoselov, M. Lotya, J.N. Coleman, M.P. Halsall, High-pressure Raman spectroscopy of graphene. *Phys. Rev. B* **80**, 073408 (2009)
- F. Tuinstra, J.L. Koenig, Raman spectrum of graphite. *J. Chem. Phys.* **53**, 1126–1130 (1970)
- F. TuzJohra, M.J. Lee, W.G. Jung, Solution-based fabrication of a graphene–ZnO nanocomposite. *J. Sol–Gel Sci. Technol.* **66**, 481–487 (2013)
- T. Sakthivel, V. Gunasekaran, S.J. Kim, Effect of oxygenated functional groups on the photoluminescence properties of graphene–oxide nanosheets. *Mater. Sci. Semicond. Process.* **19**, 174–178 (2014)
- F. Han, S. Yang, W. Jing, Z. Jiang, H. Liu, L. Li, A study on near-UV blue photoluminescence in graphene oxide prepared by Langmuir–Blodgett method. *Appl. Surf. Sci.* **345**, 18–23 (2015)
- T. Terasawa, K. Saiki, Growth of graphene on Cu by plasma enhanced chemical vapor deposition. *Carbon* **50**, 869–874 (2012)
- R.F. Elsupikhe, K. Shameli, M.B. Ahmad, Effect of ultrasonic radiation's times to the control size of silver nanoparticles in κ -carrageenan. *Res. Chem. Intermed.* **41**, 8829–8838 (2015)
- R. Karimzadeh, N. Mansour, Concentration effects on the thermo-optical properties of colloidal silver nanoparticles. *Opt. Laser Technol.* **42**, 783–789 (2010)
- J. Tauc, R. Grigorovici, A. Vancu, Optical properties and electronic structure of amorphous germanium. *Phys. Status solidi* **15**, 627 (1996)
- J.I. Pankove, *Optical Process in Semiconductors*, 1st edn. (Prentice Hall Inc., New Jersey, 1971)
- M. Sheik-Bahae, A.A. Said, T.H. Wei, D.J. Hagan, E.W. Van Stryland, Sensitive measurement of optical nonlinearities using a single beam. *IEEE J.* **26**, 760–769 (1990)
- M. Sheik-Bahae, M.P. Hasselbeck, Third order optical nonlinearities. *Handb Opt.* **4**, 1–50 (2000)
- S. Couris, M. Renard, O. Faucher, B. Lavorel, R. Chauv, E. Koudoumas, X. Michaut, An experimental investigation of the nonlinear refractive index (n_2) of carbon disulfide and toluene by spectral shearing interferometry and z-scan techniques. *Chem. Phys. Lett.* **369**, 318–324 (2003)
- P. Poornesh, P.K. Hegde, G. Umesh, M.G. Manjunatha, K.B. Manjunatha, A.V. Adhikari, Nonlinear optical and optical power limiting studies on a new thiophene-based conjugated polymer in solution and solid PMMA matrix. *Opt. Laser Technol.* **42**, 230–236 (2010)
- B. Anand, S.R. Krishnan, R. Podila, S.S. Sankara Sai, A.M. Raocde, R. Philip, The role of defects in the nonlinear optical absorption behavior of carbon and ZnO nanostructures. *Phys. Chem. Chem. Phys.* **16**, 8168–8177 (2014)
- R.W. Hellwarth, Third-order optical susceptibilities of liquids and solids. *Prog. Quant. Electron.* **5**, 1–68 (1979)
- R. Coso, J. Solis, Relation between nonlinear refractive index and third-order susceptibility in absorbing media. *J. Opt. Soc. Am. B* **21**, 640–644 (2004)